

# Constraints on dark energy dynamics and spatial curvature from Hubble parameter and baryon acoustic oscillation data

Joseph Ryan<sup>1</sup><sup>\*</sup>, Sanket Doshi<sup>2,1</sup><sup>†</sup>, and Bharat Ratra<sup>1</sup><sup>‡</sup>

<sup>1</sup>*Department of Physics, Kansas State University, 116 Cardwell Hall, Manhattan, KS 66506, USA*

<sup>2</sup>*Department of Physics, Indian Institute of Technology Bombay, Mumbai 400076, India*

Last updated 20XX YYY ZZ; in original form 20XX YYY ZZ

## ABSTRACT

We use available baryon acoustic oscillation distance measurements and Hubble parameter data to constrain the cosmological constant  $\Lambda$ , dynamical dark energy, and spatial curvature in simple cosmological models. We find that the consensus spatially flat  $\Lambda$ CDM model provides a reasonable fit to the data, but depending on the Hubble constant prior and cosmological model, it can be up to  $2\sigma$  away from the best-fit model, which can favor mild dark energy dynamics or mildly closed spatial hypersurfaces.

**Key words:** cosmological parameters – dark energy – cosmology: observations

## 1 INTRODUCTION

It is widely accepted that the universe is undergoing accelerated expansion today. The consensus cosmological model,  $\Lambda$ CDM, posits that this acceleration is driven by the spatially homogeneous, constant dark energy density  $\rho_\Lambda$  of the cosmological constant  $\Lambda$  (Peebles 1984).<sup>1</sup> The consensus  $\Lambda$ CDM model assumes flat spatial hypersurfaces, but observations don't rule out mildly curved spatial hypersurfaces; observations also do not rule out the possibility that the dark energy density varies slowly with time. In this paper we examine, in addition to the general (not necessarily spatially flat)  $\Lambda$ CDM model, the XCDM parametrization of dynamical dark energy, and the  $\phi$ CDM model in which a scalar field  $\phi$  is the dynamical dark energy.<sup>2</sup> In the XCDM and  $\phi$ CDM cases we allow for both vanishing and non-vanishing spatial curvature. Details of the three

models we study are summarized in Sec. 2, and more information can be found in Farooq (2013).

Ooba et al. (2018) have recently shown that, in the spatially flat case, the Planck 2015 CMB anisotropy data from Planck Collaboration (2016) (and some baryon acoustic oscillation distance measurements) weakly favor the XCDM parametrization and the  $\phi$ CDM model of dynamical dark energy over the  $\Lambda$ CDM consensus model. The XCDM case results have been confirmed by Park & Ratra (2018a) for a much bigger compilation of cosmological data, including most available Type Ia supernova apparent magnitude observations, BAO distance measurements, growth factor data, and Hubble parameter observations.<sup>3</sup> Also, spatially flat XCDM and  $\phi$ CDM both reduce the tension between CMB anisotropy and weak gravitational lensing estimates of  $\sigma_8$ , the rms fractional energy density inhomogeneity averaged over  $8 h^{-1}$  Mpc radius spheres (Ooba et al. 2018; Park & Ratra 2018a).<sup>4</sup>

In non-flat models nonzero spatial curvature provides an additional length scale which invalidates usage of the power-law power spectrum for energy density inhomogeneities in the non-flat case (as was assumed in the analysis of non-flat models in Planck Collaboration 2016). Non-flat inflation models (Gott 1982; Hawking 1984; Ratra 1985) provide the only known physically-consistent

\* E-mail: jwryan@phys.ksu.edu

† E-mail: sanketdoshik2@iitb.ac.in

‡ E-mail: ratra@phys.ksu.edu

<sup>1</sup> For reviews of the accelerated cosmological expansion and of the  $\Lambda$ CDM model, see Ratra & Vogeley (2008), Martin (2012), Brax (2018), and Luković et al. (2018). In this model, cold dark matter (CDM) is the second largest contributor to the current energy budget and, with non-relativistic baryonic matter, powered the decelerating cosmological expansion at earlier times.

<sup>2</sup> While cosmic microwave background (CMB) anisotropy data provide the most restrictive constraints on cosmological parameters, many other measurements have been used to constrain the XCDM parametrization and the  $\phi$ CDM model (see, e.g., Samushia et al. 2007, Yashar et al. 2009, Samushia & Ratra 2010, Chen & Ratra 2011b, Campanelli et al. 2012, Pavlov et al. 2014, Avsajanishvili et al. 2015, Sola Peracaula et al. 2016, Sola et al. 2017a; Solà et al. 2017b,c,d, Avsajanishvili et al. 2017, Gómez-Valent & Solà 2017, Zhai et al. 2017, Mehrabi & Basilakos 2018, Sangwan et al. 2018).

<sup>3</sup> For earlier indications favoring dynamical dark energy over the  $\Lambda$ CDM consensus model, based on smaller compilations of data, see Sahni et al. (2014), Ding et al. (2015), Solà et al. (2015), Zheng et al. (2016), Solà et al. (2017d), Sola Peracaula et al. (2016), Solà et al. (2017b), Zhao et al. (2017), Sola et al. (2017a), Zhang et al. (2017a), Solà et al. (2017c), Gómez-Valent & Solà (2017), Cao et al. (2017), and Gómez-Valent & Solà (2018). However, more recent analyses, based on bigger compilations of data, do not support the significant evidence for dynamical dark energy indicated in some of the earlier analyses (Ooba et al. 2018; Park & Ratra 2018a).

<sup>4</sup> Here  $h$  is the Hubble constant in units of  $100 \text{ km s}^{-1} \text{ Mpc}^{-1}$ .

mechanism for generating energy density inhomogeneities in the non-flat case; the resulting open and closed model power spectra are not power laws (Ratra & Peebles 1994, 1995; Ratra 2017). Using these power spectra, Ooba et al. (2017a) have found that the Planck 2015 CMB anisotropy data in combination with a few BAO distance measurements no longer rule out the non-flat  $\Lambda$ CDM case (unlike the earlier Planck Collaboration (2016) analyses based on the incorrect assumption of a power-law power spectrum in the non-flat model).<sup>5</sup> Park & Ratra (2018b) confirmed these results for a bigger compilation of cosmological data.<sup>6</sup>

Additionally, the non-flat models provide a better fit to the observed low multipole CMB anisotropy power spectrum, and do better at reconciling the CMB anisotropy and weak lensing constraints on  $\sigma_8$ , but do a worse job at fitting the observed large multipole CMB anisotropy power spectrum (Ooba et al. 2017a,b,c; Park & Ratra 2018a,b). Given the non-standard normalization of the Planck 2015 CMB anisotropy likelihood and that the flat and non-flat  $\Lambda$ CDM models are not nested, it is not possible to compute the relative goodness of fit between the flat and non-flat  $\Lambda$ CDM models quantitatively, although qualitatively the flat  $\Lambda$ CDM model provides a better fit to the current data (Ooba et al. 2017a,b,c; Park & Ratra 2018a,b).

In the analyses discussed above, the Planck 2015 CMB anisotropy data played the major role. Those authors found consistency between cosmological constraints derived using the CMB anisotropy data in combination with various non-CMB data sets. CMB anisotropy data are sensitive to the behavior of cosmological spatial inhomogeneities. Here we derive constraints on similar models from a combination of all available Hubble parameter data as well as all available radial and transverse BAO data.<sup>7</sup> Unlike the CMB anisotropy data, the  $H(z)$  and these BAO data are not sensitive to the behavior of cosmological spatial inhomogeneities.

The constraints we derive here are consistent with, but weaker than, those of the papers cited above; this provides a necessary and useful consistency test of those results. In particular, we find that the consensus flat  $\Lambda$ CDM model is a reasonable fit, in most cases, to the BAO and  $H(z)$  data we study here. However, depending somewhat on the Hubble constant prior we use, consensus flat  $\Lambda$ CDM can be  $1\sigma$  or  $2\sigma$  away from the best-fit parameter values in some cases, which can favor mild dark energy dynamics or mildly closed spatial hypersurfaces.

In Sec. 2 we provide a short summary of the models we studied. Sec. 3 presents the data that we used, and in Sec. 4 we describe the methods by which we analyzed these data. Sec. 5 describes the results of our analyses, and our conclusions are given in Sec. 6.

<sup>5</sup> Currently available non-CMB measurements do not significantly constrain spatial curvature (Farooq et al. 2015; Chen et al. 2016; Yu & Wang 2016; L’Huillier & Shafieloo 2017; Farooq et al. 2017; Wei & Wu 2017; Rana et al. 2017; Yu et al. 2018; Mitra et al. 2017).

<sup>6</sup> Similar conclusions hold in the non-flat dynamical dark energy XCDM and  $\phi$ CDM cases (Ooba et al. 2017b,c; Park & Ratra 2018a).

<sup>7</sup> The  $H(z)$  and radial BAO data provide a unique measure of the cosmological expansion rate over a wide redshift range, up to almost  $z = 2.4$ , well past the cosmological deceleration-acceleration transition redshift. These data show evidence for this transition and can be used to measure the redshift of the transition (Farooq & Ratra 2013; Farooq et al. 2013; Capozziello et al. 2014; Moresco et al. 2016; Farooq et al. 2017; Yu et al. 2018; Jesus et al. 2017; Haridasu et al. 2018).

## 2 MODELS

The models we examine in this paper are characterized by their expansion rate as a function of redshift  $z$ ,

$$E(z) = \frac{H(z)}{H_0}. \quad (1)$$

Here  $H(z)$  is the Hubble parameter and  $H_0 \equiv H(0)$  is the Hubble constant.

In the  $\Lambda$ CDM model dark energy is a constant vacuum energy density with negative pressure, equivalent to an ideal fluid with equation of state parameter

$$w = \frac{p_b}{\rho_b} = -1. \quad (2)$$

Here  $p_b$  and  $\rho_b$  are the homogeneous parts of the pressure and energy density, respectively. The expansion rate can be written in terms of the density parameters

$$E(z) = \sqrt{\Omega_{m0}(1+z)^3 + (1 - \Omega_{m0} - \Omega_\Lambda)(1+z)^2 + \Omega_\Lambda}, \quad (3)$$

where  $\Omega_{m0}$  is the current value of the non-relativistic matter density parameter,  $\Omega_\Lambda$  is the cosmological constant density parameter, and  $\Omega_{k0} = 1 - \Omega_{m0} - \Omega_\Lambda$  (which is nonzero in general) is the current value of the spatial curvature density parameter.<sup>8</sup> The  $\Lambda$ CDM model is characterized by two parameters:  $p = (\Omega_{m0}, \Omega_\Lambda)$ .

In the XCDM parametrization of dark energy,  $w = w_X$  where  $w_X$  is a negative constant (in general  $w_X \neq -1$ ). Hence

$$E(z) = \sqrt{\Omega_{m0}(1+z)^3 + \Omega_{k0}(1+z)^2 + \Omega_{X0}(1+z)^{3(1+w_X)}}, \quad (4)$$

where  $\Omega_{X0}$  is the current value of the dark energy density. In contrast to  $\Lambda$ CDM, the dark energy density parameter  $\Omega_{X0}(1+z)^{3(1+w_X)}$  varies with time.<sup>9</sup> If, however,  $w_X = -1$ , then XCDM reduces to  $\Lambda$ CDM, with  $\Omega_{X0} = \Omega_\Lambda$ . In general, the XCDM model has three free parameters:  $p = (\Omega_{m0}, \Omega_{k0}, w_X)$ . We shall also consider spatially flat XCDM, with  $p = (\Omega_{m0}, w_X)$ .

The  $\phi$ CDM model (Peebles & Ratra 1988; Ratra & Peebles 1988; Farooq 2013; Pavlov et al. 2013) provides a simple, physically consistent description of dynamical dark energy. In this model, the dark energy is a scalar field  $\phi$  with a potential energy density given by

$$V(\phi) = \frac{1}{2} \kappa m_p^2 \phi^{-\alpha}. \quad (5)$$

Here  $\alpha > 0$ ,  $m_p^2 \equiv G^{-1}$ ,  $G$  is the gravitational constant, and

$$\kappa = \frac{8}{3} \left( \frac{\alpha + 4}{\alpha + 2} \right) \left[ \frac{2}{3} \alpha (\alpha + 2) \right]^{-\alpha/2}. \quad (6)$$

The spatially homogeneous part of the scalar field obeys

$$\ddot{\phi} + 3 \frac{\dot{a}}{a} \dot{\phi} - \frac{1}{2} \kappa \alpha m_p^2 \phi^{-\alpha-1} = 0, \quad (7)$$

<sup>8</sup> Here, and in the other models we study, we ignore the contributions from CMB photons and neutrinos, which are very small at the redshifts of the data we use.

<sup>9</sup> In the XCDM parametrization, the energy density and pressure of the dark energy fluid,  $\rho_{Xb}(t)$  and  $p_{Xb}(t)$ , are space-independent functions of time. When  $\rho_{Xb}(t)$  is negative, this is an inconsistent parametrization that is rendered consistent by assuming a constant speed of acoustic inhomogeneities (typically  $c_{sX} = 1$ ). The BAO and  $H(z)$  data we consider only constrain the spatially homogeneous part of the cosmological models.

**Table 1.** BAO data.  $D_M(r_s, \text{fid}/r_s)$  and  $D_V(r_s, \text{fid}/r_s)$  have units of Mpc, while  $H(z)(r_s/r_s, \text{fid})$  has units of  $\text{km s}^{-1}\text{Mpc}^{-1}$  and  $r_s$  has units of Mpc.

$z$	Measurement	Value	$\sigma$	Ref.
0.38	$D_M(r_s, \text{fid}/r_s)$	1518	22	Alam et al. (2017)
0.51	$D_M(r_s, \text{fid}/r_s)$	1977	27	Alam et al. (2017)
0.61	$D_M(r_s, \text{fid}/r_s)$	2283	32	Alam et al. (2017)
0.38	$H(z)(r_s/r_s, \text{fid})$	81.5	1.9	Alam et al. (2017)
0.51	$H(z)(r_s/r_s, \text{fid})$	90.4	1.9	Alam et al. (2017)
0.61	$H(z)(r_s/r_s, \text{fid})$	97.3	2.1	Alam et al. (2017)
0.106	$r_s/D_V$	0.336	0.015	Beutler et al. (2011)
0.15	$D_V(r_s, \text{fid}/r_s)$	664	25	Ross et al. (2015)
1.52	$D_V(r_s, \text{fid}/r_s)$	3855	170	Ata et al. (2018)
2.33	$\frac{(D_H)^{0.7}(D_M)^{0.3}}{r_s}$	13.94	0.35	Bautista et al. (2017)
2.36	$c/(r_s H(z))$	9.0	0.3	Font-Ribera et al. (2014)

where  $a = a(t)$  is the scale factor, and an overdot denotes differentiation with respect to time. This, together with the first Friedmann equation,

$$\left(\frac{\dot{a}}{a}\right)^2 = \frac{8\pi G}{3}(\rho_m + \rho_\phi) - \frac{k}{a^2}, \quad (8)$$

and

$$\rho_\phi = \frac{1}{2}\dot{\phi}^2 + V(\phi), \quad (9)$$

determines the dynamics of the field. In eq. (8),  $\rho_m$  is the non-relativistic matter density,  $\rho_\phi$  is the scalar field energy density, and  $k = 0, +1, -1$  for flat, closed, and open spatial hypersurfaces, respectively.

The dark energy equation of state parameter of  $\phi$ CDM is

$$w_\phi = \frac{p_\phi}{\rho_\phi} = \frac{\frac{1}{2}\dot{\phi}^2 - V(\phi)}{\frac{1}{2}\dot{\phi}^2 + V(\phi)}, \quad (10)$$

which, unlike in the  $\Lambda$ CDM and XCDM models, changes with time. The expansion rate in the  $\phi$ CDM model is

$$E(z) = \sqrt{\Omega_{m0}(1+z)^3 + \Omega_{k0}(1+z)^2 + \Omega_\phi(z, \alpha)}, \quad (11)$$

where

$$\Omega_\phi(z, \alpha) \equiv \frac{8\pi G\rho_\phi}{3H_0^2}. \quad (12)$$

In contrast to  $\Omega_\chi$ ,  $\Omega_\phi$  is not an explicit function of a power of  $(1+z)$ ; it must be determined numerically.

In general, the  $\phi$ CDM model has three free parameters:  $p = (\Omega_{m0}, \Omega_{k0}, \alpha)$ . We also consider spatially flat  $\phi$ CDM with  $p = (\Omega_{m0}, \alpha)$ .

### 3 DATA

BAO<sup>10</sup> provide observers with a ‘‘standard ruler’’ which can be used to measure cosmological distances. These distances can be

<sup>10</sup> See Bassett & Hlozek (2010) for a review.

**Table 2.**  $H(z)$  data.  $H(z)$  and  $\sigma_H$  have units of  $\text{km s}^{-1}\text{Mpc}^{-1}$ .

$z$	$H(z)$	$\sigma_H$	Ref.
0.07	69	19.6	Zhang et al. (2014)
0.09	69	12	Simon et al. (2005)
0.12	68.6	26.2	Zhang et al. (2014)
0.17	83	8	Simon et al. (2005)
0.179	75	4	Moresco et al. (2012)
0.199	75	5	Moresco et al. (2012)
0.20	72.9	29.6	Zhang et al. (2014)
0.27	77	14	Simon et al. (2005)
0.28	88.8	36.6	Zhang et al. (2014)
0.352	83	14	Moresco et al. (2012)
0.3802	83	13.5	Moresco et al. (2016)
0.4	95	17	Simon et al. (2005)
0.4004	77	10.2	Moresco et al. (2016)
0.4247	87.1	11.2	Moresco et al. (2016)
0.4497	92.8	12.9	Moresco et al. (2016)
0.47	89	50	Ratsimbazafy et al. (2017)
0.4783	80.9	9	Moresco et al. (2016)
0.48	97	62	Stern et al. (2010)
0.593	104	13	Moresco et al. (2012)
0.68	92	8	Moresco et al. (2012)
0.781	105	12	Moresco et al. (2012)
0.875	125	17	Moresco et al. (2012)
0.88	90	40	Stern et al. (2010)
0.90	117	23	Simon et al. (2005)
1.037	154	20	Moresco et al. (2012)
1.3	168	17	Simon et al. (2005)
1.363	160	33.6	Moresco (2015)
1.43	177	18	Simon et al. (2005)
1.53	140	14	Simon et al. (2005)
1.75	202	40	Simon et al. (2005)
1.965	186.5	50.4	Moresco (2015)

computed in a given cosmological model, so measurements of them can be used to constrain the parameters of the model in question. The BAO distance measurements we use are listed in Table 1.

The transverse co-moving distance is

$$D_M(z) = \begin{cases} D_C & \text{if } \Omega_{k0} = 0, \\ \frac{c}{H_0\sqrt{|\Omega_{k0}|}} \sinh\left[\sqrt{|\Omega_{k0}|}\frac{D_C H_0}{c}\right] & \text{if } \Omega_{k0} > 0, \\ \frac{c}{H_0\sqrt{|\Omega_{k0}|}} \sin\left[\sqrt{|\Omega_{k0}|}\frac{D_C H_0}{c}\right] & \text{if } \Omega_{k0} < 0, \end{cases} \quad (13)$$

where

$$D_H = \frac{c}{H(z)}, \quad (14)$$

$$D_C = \frac{c}{H_0} \int_0^z \frac{dz'}{E(z')}, \quad (15)$$

and the volume-averaged angular diameter distance is

$$D_V(z) = \left[ \frac{cz}{H_0} \frac{D_M^2(z)}{E(z)} \right]^{1/3} \quad (16)$$

(Hogg 1999; Farooq 2013). All of the measurements in Table 1 are scaled by the size of the sound horizon at the drag epoch ( $r_s$ ). This quantity is (see Eisenstein & Hu 1998 for a derivation):

$$r_s = \frac{2}{3k_{\text{eq}}} \sqrt{\frac{6}{R_{\text{eq}}}} \ln \left[ \frac{\sqrt{1+R_d} + \sqrt{R_d + R_{\text{eq}}}}{1 + \sqrt{R_{\text{eq}}}} \right] \quad (17)$$

where  $R_d \equiv R(z_d)$  and  $R_{\text{eq}} \equiv R(z_{\text{eq}})$  are the values of  $R$ , the ratio of the baryon to photon momentum density,

$$R = \frac{3\rho_b}{4\rho_\gamma} \quad (18)$$

at the drag epoch and matter-radiation equality epoch, respectively. Here  $k_{\text{eq}}$  is the scale of the particle horizon at the matter-radiation equality epoch, and  $\rho_b$  and  $\rho_\gamma$  are the baryon and photon mass densities. In our analyses, where appropriate, the original data listed in Table 1 have been rescaled to a fiducial sound horizon  $r_{s,\text{fid}} = 147.60$  Mpc (from Table 4, column 2, of Planck Collaboration 2016).

In Table 2 we list 31  $H(z)$  measurements determined using the cosmic chronometric technique (see e.g. Moresco 2015 for a discussion of cosmic chronometers). This compilation is the same as the cosmic chronometric  $H(z)$  data used in Yu et al. (2018).

## 4 METHODS

To determine the values of the best-fit parameters, we minimized

$$\chi^2(p) \equiv -2 \ln \mathcal{L}(p), \quad (19)$$

where  $\mathcal{L}$  is the likelihood function and  $p$  is the set of parameters of the model under consideration. If the likelihood function  $\mathcal{L}(p, \nu)$  depends on an uninteresting nuisance parameter  $\nu$  with a probability distribution  $\pi(\nu)$ , we marginalize the likelihood function by integrating  $\mathcal{L}(p, \nu)$  over  $\nu$

$$\mathcal{L}(p) = \int \mathcal{L}(p, \nu) \pi(\nu) d\nu. \quad (20)$$

In our  $H(z)$  analyses  $H_0$  is a nuisance parameter. We assumed a Gaussian distribution for  $H_0$

$$\pi(H_0) = \frac{1}{\sqrt{2\pi\sigma_{H_0}^2}} \exp \left[ -\frac{(H_0 - \bar{H}_0)^2}{2\sigma_{H_0}^2} \right] \quad (21)$$

and marginalized over it. We considered two cases:  $\bar{H}_0 \pm \sigma_{H_0} = 68 \pm 2.8$  km s<sup>-1</sup> Mpc<sup>-1</sup> and  $\bar{H}_0 \pm \sigma_{H_0} = 73.24 \pm 1.74$  km s<sup>-1</sup> Mpc<sup>-1</sup>.<sup>11</sup>

<sup>11</sup> The lower value,  $68 \pm 2.8$  km s<sup>-1</sup> Mpc<sup>-1</sup> is the most recent median statistics estimate of the Hubble constant (Chen & Ratra 2011a). It is consistent with earlier median statistics estimates (Gott et al. 2001; Chen et al. 2003).

Most of the data we analyzed are uncorrelated, however six of the data points (those from Alam et al. 2017), are correlated. For uncorrelated data points,

$$\chi^2(p) = \sum_{i=1}^N \frac{[A_{\text{th}}(p; z_i) - A_{\text{obs}}(z_i)]^2}{\sigma_i^2}, \quad (22)$$

where  $A_{\text{th}}(p; z_i)$  are the model predictions at redshifts  $z$ , and  $A_{\text{obs}}(z_i)$  and  $\sigma_i$  are the central values and error bars of the measurements listed in Table 2 and the last five lines of Table 1. The correlated data (the first six entries in Table 1) require

$$\chi^2(p) = [\vec{A}_{\text{th}}(p) - \vec{A}_{\text{obs}}]^T C^{-1} [\vec{A}_{\text{th}}(p) - \vec{A}_{\text{obs}}] \quad (23)$$

where  $C^{-1}$  is the inverse of the covariance matrix

$$C = \begin{bmatrix} 484.0 & 9.530 & 295.2 & 4.669 & 140.2 & 2.402 \\ 9.530 & 3.610 & 7.880 & 1.759 & 5.983 & 0.9205 \\ 295.2 & 7.880 & 729.0 & 11.93 & 442.4 & 6.866 \\ 4.669 & 1.759 & 11.93 & 3.610 & 9.552 & 2.174 \\ 140.2 & 5.983 & 442.4 & 9.552 & 1024 & 16.18 \\ 2.402 & 0.9205 & 6.866 & 2.174 & 16.18 & 4.410 \end{bmatrix} \quad (24)$$

(Alam et al. 2017).  $\vec{A}_{\text{obs}}$  (in eq. 23) are the measurements in the first six lines of Table 1.

In addition to  $\chi^2$ , we also used the Bayes Information Criterion

$$\text{BIC} \equiv \chi_{\text{min}}^2 + k \ln N \quad (25)$$

and the Akaike Information Criterion

$$\text{AIC} \equiv \chi_{\text{min}}^2 + 2k \quad (26)$$

(Liddle 2007). In these equations  $\chi_{\text{min}}^2$  is the minimum value of  $\chi^2$ ,  $k$  is the number of parameters of the given model, and  $N$  is the number of data points. BIC and AIC provide means to compare models with different numbers of parameters; they penalize models with a higher  $k$  in favor of those with a lower  $k$ , in effect enforcing Occam's Razor in the model selection process.

To determine the confidence intervals  $r_n$  on the 1d best-fit parameters, we computed one-sided limits  $r_n^\pm$  by using

$$\frac{\int_{\bar{p}}^{r_n^\pm} \mathcal{L}(p) dp}{\int_{\bar{p}}^{\pm\infty} \mathcal{L}(p) dp} = \sigma_n, \quad (27)$$

where  $\bar{p}$  is the point at which  $\mathcal{L}(p)$  has its maximum value, such that  $n = 1, 2$  and  $\sigma_1 = 0.6827$ ,  $\sigma_2 = 0.9545$ . Because the one-dimensional likelihood function is not guaranteed to be symmetric about  $\bar{p}$ , we compute the upper and lower confidence intervals separately. In the  $\Lambda$ CDM model, for example, the 1-sigma confidence intervals on  $\Omega_{m0}$  are computed by first integrating the likelihood function  $\mathcal{L}(\Omega_{m0}, \Omega_\Lambda)$  over  $\Omega_\Lambda$  to obtain a marginalized likelihood function that only depends on  $\Omega_{m0}$ ,

$$\int_0^1 \mathcal{L}(\Omega_{m0}, \Omega_\Lambda) d\Omega_\Lambda = \mathcal{L}(\Omega_{m0}), \quad (28)$$

It is also consistent with many other recent measurements of  $H_0$  (Planck Collaboration 2016; L'Huillier & Shafieloo 2017; Chen et al. 2017; Wang et al. 2017; Lin & Ishak 2017; Haridasu et al. 2017; Gómez-Valent & Amendola 2018; Yu et al. 2018; Park & Ratra 2018a; Haridasu et al. 2018). The higher value,  $73.24 \pm 1.74$  km s<sup>-1</sup> Mpc<sup>-1</sup>, comes from a local expansion rate estimate (Riess et al. 2016). Other local expansion rate estimates find slightly lower  $H_0$ 's with larger error bars (Rigault et al. 2015; Zhang et al. 2017b; Dhawan et al. 2018; Fernández Arenas et al. 2018).

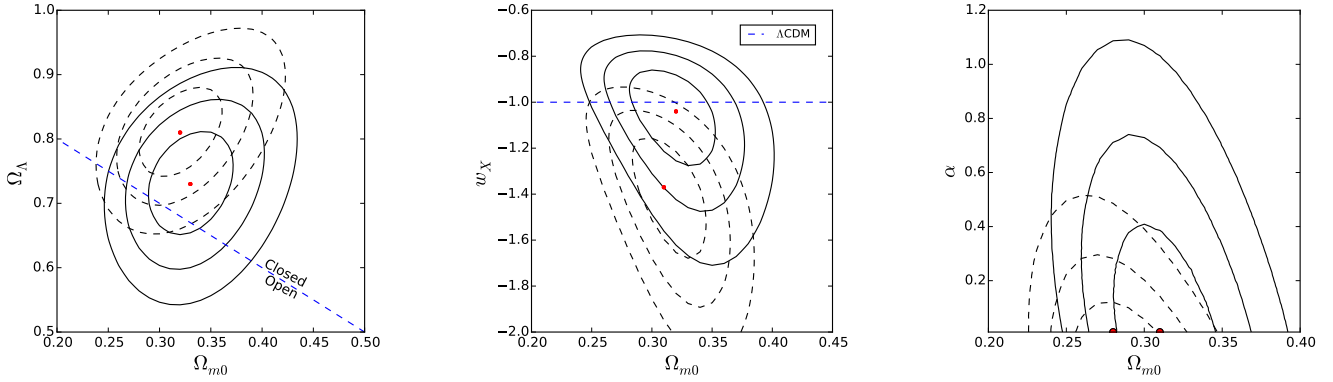


**Figure 1.** Confidence contours for 2-parameter models. Solid (dashed) 1, 2, and  $3\sigma$  contours correspond to  $\bar{H}_0 \pm \sigma_{H_0} = 68 \pm 2.8$  ( $73.24 \pm 1.74$ )  $\text{km s}^{-1} \text{Mpc}^{-1}$  prior, and the red dots indicate the location of the best-fit point in each prior case. Left:  $\Lambda\text{CDM}$ . The blue dashed line indicates the spatially flat  $\Lambda\text{CDM}$  model; points above (below) the line correspond to models with closed (open) spatial hypersurfaces. Center: flat XCDM. The blue dashed line (for which  $w_X = -1$ ) demarcates the flat  $\Lambda\text{CDM}$  case. Right: flat  $\phi\text{CDM}$ . The horizontal  $\alpha = 0$  axis corresponds to the flat  $\Lambda\text{CDM}$  model. Color online.

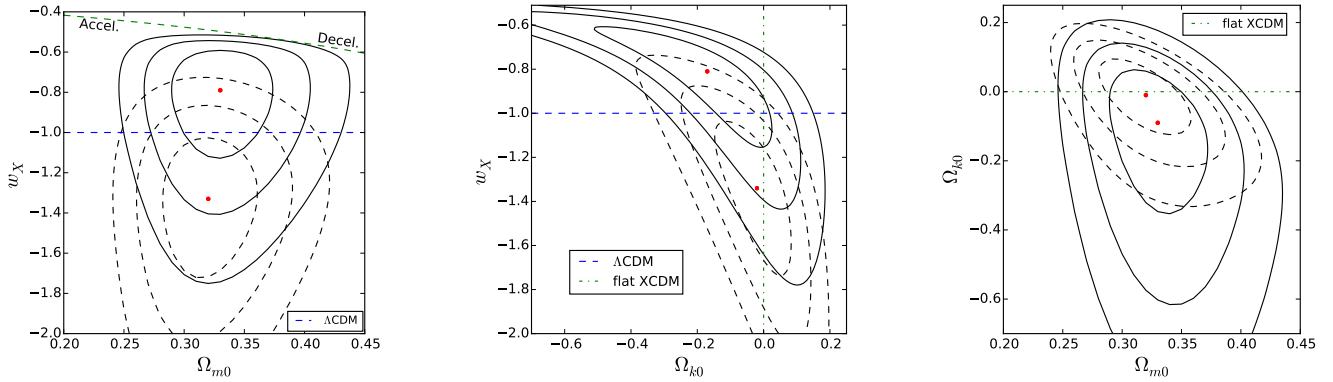


**Figure 2.** Confidence contours for 3-parameter XCDM. Solid (dashed) 1, 2, and  $3\sigma$  contours correspond to  $\bar{H}_0 \pm \sigma_{H_0} = 68 \pm 2.8$  ( $73.24 \pm 1.74$ )  $\text{km s}^{-1} \text{Mpc}^{-1}$  prior, and the red dots indicate the location of the best-fit point in each prior case. Left:  $\Omega_{k0}$  marginalized. The blue dashed line indicates the  $\Lambda\text{CDM}$  model. Points above (below) the green dot-dashed curve near the top of the panel correspond to models with late-time (decelerating) accelerating expansion. Center:  $\Omega_{m0}$  marginalized. The horizontal blue dashed line (for which  $w_X = -1$ ) demarcates the  $\Lambda\text{CDM}$  case, and the vertical green dot-dashed line demarcates the spatially flat XCDM case. Right:  $w_X$  marginalized. The horizontal green dot-dashed line indicates the spatially flat XCDM case. Color online.

and then inserting this marginalized likelihood function into eq. (27).

The ranges over which we marginalized the parameters of the  $\Lambda\text{CDM}$  model were  $0 \leq \Omega_\Lambda \leq 1$  and  $0 \leq \Omega_{m0} \leq 1$ . For the spatially flat XCDM parametrization, we used  $-2 \leq w_X \leq 0$  and  $0 \leq \Omega_{m0} \leq 1$ , and for the spatially flat  $\phi\text{CDM}$  model we used  $0.01 \leq \alpha \leq 1.4$  and  $0.20 \leq \Omega_{m0} \leq 0.50$ . For 3-parameter XCDM, we used  $-0.7 \leq \Omega_{k0} \leq 0.2$ ,  $0.20 \leq \Omega_{m0} \leq 0.45$ , and  $-2.00 \leq w_X \leq -0.33$ . For the 3-parameter  $\phi\text{CDM}$  model we considered  $-0.5 \leq \Omega_{k0} \leq 0.5$ ,  $0.01 \leq \Omega_{m0} \leq 0.99$ , and  $0.01 \leq \alpha \leq 5$ .<sup>12</sup>

We analyzed the data with two independent Python codes, written by S.D. and J.R., that produced almost identical results

<sup>12</sup> We chose smaller marginalization ranges of  $\Omega_{m0}$  in the 3-parameter XCDM parametrization and the 2-parameter  $\phi\text{CDM}$  model for computational efficiency. The marginalization range of  $\alpha$  in the 2- and 3-parameter cases of the  $\phi\text{CDM}$  model excludes  $\alpha = 0$ , and that for  $\Omega_{m0}$  in the 3-parameter  $\phi\text{CDM}$  case excludes  $\Omega_{m0} = 0, 1$ , because our codes ran into difficulties at these points.

in the 2-parameter cases and the 3-parameter XCDM model, and results that agreed to within 1% in the 3-parameter  $\phi\text{CDM}$  case.

## 5 RESULTS

The confidence contours for the models we considered are shown in Figs. 1, 2, and 3. The solid black contours indicate the  $\bar{H}_0 = 68 \pm 2.8$   $\text{km s}^{-1} \text{Mpc}^{-1}$  prior constraints, the dashed black contours indicate the  $H_0 = 73.24 \pm 1.74$   $\text{km s}^{-1} \text{Mpc}^{-1}$  prior constraints, and the red dots indicate the best-fit point in each prior case. Our results for the parameter values of the unmarginalized and marginalized cases are collected in Tables 3-6, along with their  $\chi^2$ , AIC, and BIC values. Wherever  $\Delta\chi^2$ ,  $\Delta\text{AIC}$ , and  $\Delta\text{BIC}$  are given, these are computed relative to the  $\chi^2$ , AIC, and BIC of the corresponding  $\Lambda\text{CDM}$  model of each prior case.

In the 2-parameter case, the model with the lowest value of  $\chi^2$  is  $\Lambda\text{CDM}$  if the prior on  $H_0$  is chosen to be  $\bar{H}_0 = 68 \pm 2.8$   $\text{km s}^{-1} \text{Mpc}^{-1}$ . If, on the other hand, the  $H_0$  prior is chosen

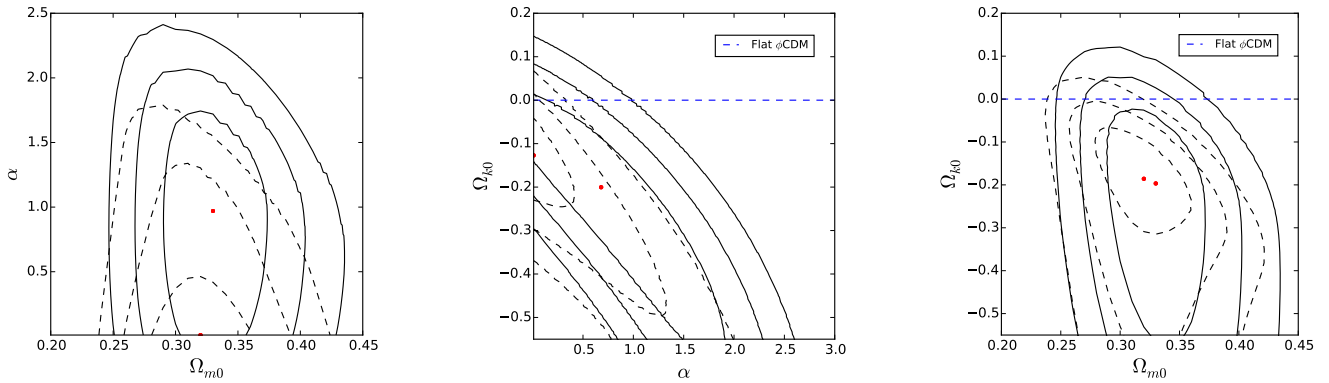


**Figure 3.** Confidence contours for 3-parameter  $\phi$ CDM. Solid (dashed) 1, 2, and  $3\sigma$  contours correspond to  $\bar{H}_0 \pm \sigma_{H_0} = 68 \pm 2.8$  ( $73.24 \pm 1.74$ )  $\text{km s}^{-1} \text{Mpc}^{-1}$  prior, and the red dots indicate the location of the best-fit point in each prior case. Left:  $\Omega_{k0}$  marginalized. The horizontal  $\alpha = 0$  axis corresponds to the  $\Lambda$ CDM model and the next panel correspond to the spatially flat  $\phi$ CDM case. Right:  $\alpha$  marginalized. Color online.

**Table 3.** Best-fit values for 2-parameter models.  $\Delta\chi^2$  is evaluated relative to  $\chi^2$  of  $\Lambda$ CDM for each  $H_0$  prior.

$H_0$ prior ( $\text{km s}^{-1} \text{Mpc}^{-1}$ )	Model	$\Omega_{m0}$	$\Omega_{\Lambda 0}$	$w_X$	$\alpha$	$\chi^2$	$\Delta\chi^2$	AIC	BIC
$68 \pm 2.8$	$\Lambda$ CDM	0.33	0.73	-	-	25.50	0.00	29.50	32.98
	flat XCDM	0.32	-	-1.04	-	26.34	0.84	30.34	33.82
	flat $\phi$ CDM	0.31	-	-	0.01	26.43	0.93	30.43	33.91
$73.24 \pm 1.74$	$\Lambda$ CDM	0.32	0.81	-	-	30.06	0.00	34.06	37.54
	flat XCDM	0.31	-	-1.37	-	27.09	-2.97	31.09	34.57
	flat $\phi$ CDM	0.28	-	-	0.01	34.99	4.93	38.99	42.47

to be  $\bar{H}_0 = 73.24 \pm 1.74 \text{ km s}^{-1} \text{Mpc}^{-1}$  then the spatially flat XCDM parametrization has the lowest value of  $\chi^2$ . These models also have lower AIC and BIC values than the 3-parameter XCDM parametrization and the 3-parameter  $\phi$ CDM model (see Tables 3 and 4). On the other hand, the 3-parameter models typically have a lower  $\chi^2$  than the 2-parameter  $\Lambda$ CDM case. These differences, however, are not statistically significant. Focusing on the  $\bar{H}_0 = 68 \pm 2.8 \text{ km s}^{-1} \text{Mpc}^{-1}$  prior case, the  $\chi^2$  differences indicate that the non-flat  $\phi$ CDM model and non-flat XCDM parametrization provide a  $0.97\sigma$  and  $0.85\sigma$  better fit to the data, respectively, while from  $\Delta\text{AIC}$  we find that these two models are 59% and 53% as probable as the 2-parameter  $\Lambda$ CDM model, respectively.

In Table 5 (6), we list the  $1\sigma$  and  $2\sigma$  confidence intervals on the parameters of each of the 2-parameter (3-parameter) models. We obtained these by marginalizing the 2-parameter (3-parameter) likelihood function as described in Sec. 4. The best-fit points in these tables correspond to the maximum value of the relevant one-dimensional marginalized likelihood function. Table 3 (4) lists the corresponding two-dimensional (three-dimensional) best-fit points.

From the figures and tables, we see that the spatially flat  $\Lambda$ CDM model is a reasonable fit to the  $H(z)$  and BAO data we use. In particular, from the figures, for the  $\bar{H}_0 \pm \sigma_{H_0} = 68 \pm 2.8 \text{ km s}^{-1} \text{Mpc}^{-1}$  prior, flat  $\Lambda$ CDM is always within  $1\sigma$  of the best-fit value (except in the right panel of Fig. 3 for the non-flat  $\phi$ CDM case, where a closed model is favored over flat  $\Lambda$ CDM by a little more than  $1\sigma$ ). However, the  $\bar{H}_0 \pm \sigma_{H_0} = 73.24 \pm 1.74 \text{ km s}^{-1} \text{Mpc}^{-1}$  case favors some larger deviations from flat  $\Lambda$ CDM. For example in the middle panel of Fig. 1 for the flat XCDM model it favors a phantom model

over flat  $\Lambda$ CDM at more than  $2\sigma$ , while in the right panel of Fig. 3 for the non-flat  $\phi$ CDM case it also favors a closed model at more than  $2\sigma$ . Similar conclusions may be drawn from the parameter limits listed in Tables 5 and 6.

When both dynamical dark energy and spatial curvature are present (as opposed to cases with only dynamical dark energy or only spatial curvature) it is not as easy to constrain both parameters simultaneously. This can be seen by comparing the center and right panels of Fig. 1 to the left panels of Figs. 2 and 3, respectively. When spatial curvature is allowed to vary, the confidence contours in the 3-parameter XCDM parametrization and the  $\phi$ CDM model expand along the  $w_X$  and  $\alpha$  axes (these are the parameters that govern the dynamics of the dark energy).

The consensus model, spatially flat  $\Lambda$ CDM, is consistent with current  $H(z)$  + BAO data, but these data allow some nonzero spatial curvature. In particular, we find that the best-fit values of the parameters in the  $\Lambda$ CDM model imply a curvature density parameter of  $\Omega_{k0} = -0.06$  for the  $\bar{H}_0 \pm \sigma_{H_0} = 68 \pm 2.8 \text{ km s}^{-1} \text{Mpc}^{-1}$  prior case, and  $\Omega_{k0} = -0.13$  for the  $\bar{H}_0 \pm \sigma_{H_0} = 73.24 \pm 1.74 \text{ km s}^{-1} \text{Mpc}^{-1}$  prior case. More precisely, using the  $\Omega_{m0}$  and  $\Omega_{\Lambda}$  best-fit values and error bars for flat  $\Lambda$ CDM from Table 5, and combining the errors in quadrature, an approximate estimate is  $\Omega_{k0} = -0.06(1 \pm 1)$  and  $\Omega_{k0} = -0.13(1 \pm 0.43)$  for the  $\bar{H}_0 \pm \sigma_{H_0} = 68 \pm 2.8 \text{ km s}^{-1} \text{Mpc}^{-1}$  and  $\bar{H}_0 \pm \sigma_{H_0} = 73.24 \pm 1.74 \text{ km s}^{-1} \text{Mpc}^{-1}$  priors, with the data favoring a closed model at  $1\sigma$  in the first case and a little over  $2\sigma$  in the second. This is also true of the 3-parameter models, in which  $\Omega_{k0}$  is not *a priori* assumed to be zero (see the center and right panels of Figs. 2 and 3). While not very statistically significant,

**Table 4.** Best-fit values for 3-parameter models.  $\Delta\chi^2$ ,  $\Delta\text{AIC}$ , and  $\Delta\text{BIC}$  are evaluated relative to  $\chi^2$ , AIC, and BIC of  $\Lambda\text{CDM}$  for each  $H_0$  prior.

$H_0$ prior (km s <sup>-1</sup> Mpc <sup>-1</sup> )	Model	$\Omega_{m0}$	$\Omega_{k0}$	$w_X$	$\alpha$	$\chi^2$	$\Delta\chi^2$	AIC	$\Delta\text{AIC}$	BIC	$\Delta\text{BIC}$
$68 \pm 2.8$	XCDM	0.33	-0.16	-0.83	-	24.77	-0.73	30.77	1.27	35.98	3.01
	$\phi\text{CDM}$	0.33	-0.22	-	0.76	24.56	-0.94	30.56	1.06	35.77	2.80
$73.24 \pm 1.74$	XCDM	0.32	-0.02	-1.35	-	26.98	-3.08	32.98	-1.08	38.19	0.66
	$\phi\text{CDM}$	0.32	-0.14	-	0.01	30.12	0.06	36.12	2.06	41.33	3.80

**Table 5.**  $1\sigma$  and  $2\sigma$  parameter intervals for 2-parameter models.

$H_0$ prior (km s <sup>-1</sup> Mpc <sup>-1</sup> )	Model	Marginalization range	Best-fit	$1\sigma$	$2\sigma$
$68 \pm 2.8$	$\Lambda\text{CDM}$	$0 \leq \Omega_{\Lambda 0} \leq 1$	$\Omega_{m0} = 0.33$	$0.30 \leq \Omega_{m0} \leq 0.36$	$0.28 \leq \Omega_{m0} \leq 0.39$
		$0 \leq \Omega_{m0} \leq 1$	$\Omega_{\Lambda 0} = 0.73$	$0.68 \leq \Omega_{\Lambda 0} \leq 0.78$	$0.62 \leq \Omega_{\Lambda 0} \leq 0.84$
	flat XCDM	$-2 \leq w_X \leq 0$	$\Omega_{m0} = 0.32$	$0.30 \leq \Omega_{m0} \leq 0.34$	$0.27 \leq \Omega_{m0} \leq 0.37$
		$0 \leq \Omega_{m0} \leq 1$	$w_X = -1.03$	$-1.2 \leq w_X \leq -0.92$	$-1.4 \leq w_X \leq -0.83$
	flat $\phi\text{CDM}$	$0.01 \leq \alpha \leq 1.4$	$\Omega_{m0} = 0.32$	$0.29 \leq \Omega_{m0} \leq 0.33$	$0.27 \leq \Omega_{m0} \leq 0.35$
		$0.20 \leq \Omega_{m0} \leq 0.50$	$\alpha = 0.01$	$0.01 \leq \alpha \leq 0.29$	$0.01 \leq \alpha \leq 0.62$
$73.24 \pm 1.74$	$\Lambda\text{CDM}$	$0 \leq \Omega_{\Lambda 0} \leq 1$	$\Omega_{m0} = 0.32$	$0.30 \leq \Omega_{m0} \leq 0.35$	$0.27 \leq \Omega_{m0} \leq 0.38$
		$0 \leq \Omega_{m0} \leq 1$	$\Omega_{\Lambda 0} = 0.81$	$0.76 \leq \Omega_{\Lambda 0} \leq 0.86$	$0.72 \leq \Omega_{\Lambda 0} \leq 0.91$
	flat XCDM	$-2 \leq w_X \leq 0$	$\Omega_{m0} = 0.32$	$0.30 \leq \Omega_{m0} \leq 0.34$	$0.28 \leq \Omega_{m0} \leq 0.36$
		$0 \leq \Omega_{m0} \leq 1$	$w_X = -1.39$	$-1.58 \leq w_X \leq -1.24$	$-1.79 \leq w_X \leq -1.10$
	flat $\phi\text{CDM}$	$0.01 \leq \alpha \leq 1.4$	$\Omega_{m0} = 0.28$	$0.26 \leq \Omega_{m0} \leq 0.30$	$0.24 \leq \Omega_{m0} \leq 0.32$
		$0.20 \leq \Omega_{m0} \leq 0.50$	$\alpha = 0.01$	$0.01 \leq \alpha \leq 0.12$	$0.01 \leq \alpha \leq 0.29$

we note that these results are not inconsistent with those of [Ooba et al. \(2017a,b,c\)](#) and [Park & Ratra \(2018a,b\)](#), who found that CMB anisotropy data, in conjunction with other cosmological data, were not inconsistent with mildly closed spatial hypersurfaces.

The current data are also not inconsistent with some mild dark energy dynamics, although the size of the effect varies depending on the choice of  $H_0$  prior and whether or not  $\Omega_{k0}$  is allowed to vary as a free parameter. In the  $\phi\text{CDM}$  model, for instance,  $\alpha$  can be different from zero in the  $\bar{H}_0 \pm \sigma_{H_0} = 68 \pm 2.8$  km s<sup>-1</sup> Mpc<sup>-1</sup> prior case, but only if spatial hypersurfaces are also closed (see line 2 of Table 4).

## 6 CONCLUSIONS

We analyzed a total of 42 measurements, 31 of which consisted of uncorrelated  $H(z)$  data points, with the remainder coming from BAO observations (some correlated, some not), to constrain dark energy dynamics and spatial curvature, by determining how well these measurements can be described by three common models of dark energy:  $\Lambda\text{CDM}$ , the XCDM parametrization, and  $\phi\text{CDM}$ .

The consensus flat  $\Lambda\text{CDM}$  model is in reasonable accord with these data, but depending on the model analyzed and the  $H_0$  prior used, it can be as far as  $2\sigma$  away from the best-fit model. These data are consistent with mild dark energy dynamics as well as mildly closed spatial hypersurfaces. While these results are interesting and encouraging, more and better data are needed before we can make definitive statements about the spatial curvature of the universe and about dark energy dynamics.

## ACKNOWLEDGEMENTS

The authors wish to thank Omer Farooq and Lado Samushia for useful discussions, as well as Kumar Ayush, Rahul Govind, and Tyler Mitchell for help with computational resources and optimization. This work was supported by DOE Grant DE-SC0011840.

## REFERENCES

- Alam S., et al., 2017, *MNRAS*, **470**, 2617  
 Ata M., et al., 2018, *MNRAS*, **473**, 4773  
 Avsajanishvili O., Samushia L., Arkhipova N. A., Kahniashvili T., 2015, preprint, ([arXiv:1511.09317](#))  
 Avsajanishvili O., Huang Y., Samushia L., Kahniashvili T., 2017, preprint, ([arXiv:1711.11465](#))  
 Bassett B., Hlozek R., 2010, Baryon acoustic oscillations. p. 246  
 Bautista J. E., et al., 2017, *A&A*, **603**, A12  
 Beutler F., et al., 2011, *MNRAS*, **416**, 3017  
 Brax P., 2018, *Reports on Progress in Physics*, **81**, 016902  
 Campanelli L., Fogli G. L., Kahniashvili T., Marrone A., Ratra B., 2012, *European Physical Journal C*, **72**, 2218  
 Cao S.-L., Duan X.-W., Meng X.-L., Zhang T.-J., 2017, preprint, ([arXiv:1712.01703](#))  
 Capozziello S., Farooq O., Luongo O., Ratra B., 2014, *Phys. Rev. D*, **90**, 044016  
 Chen G., Ratra B., 2011a, *PASP*, **123**, 1127  
 Chen Y., Ratra B., 2011b, *Physics Letters B*, **703**, 406  
 Chen G., Gott III J. R., Ratra B., 2003, *PASP*, **115**, 1269  
 Chen Y., Ratra B., Biesiada M., Li S., Zhu Z.-H., 2016, *ApJ*, **829**, 61  
 Chen Y., Kumar S., Ratra B., 2017, *ApJ*, **835**, 86  
 Dhawan S., Jha S. W., Leibundgut B., 2018, *A&A*, **609**, A72

**Table 6.**  $1\sigma$  and  $2\sigma$  parameter intervals for 3-parameter models.

$H_0$ prior (km s <sup>-1</sup> Mpc <sup>-1</sup> )	Model	Marginalization range	Best-fit	$1\sigma$	$2\sigma$
$68 \pm 2.8$	XCDM	$-0.7 \leq \Omega_{k0} \leq 0.2$	$\Omega_{m0} = 0.33$ $w_X = -0.79$	$0.30 \leq \Omega_{m0} \leq 0.36$ $-1.02 \leq w_X \leq -0.67$	$0.28 \leq \Omega_{m0} \leq 0.39$ $-1.30 \leq w_X \leq -0.59$
		$0.20 \leq \Omega_{m0} \leq 0.45$	$\Omega_{k0} = -0.1$ $w_X = -0.79$	$-0.29 \leq \Omega_{k0} \leq 0.00$ $-1.02 \leq w_X \leq -0.67$	$-0.52 \leq \Omega_{k0} \leq 0.09$ $-1.30 \leq w_X \leq -0.59$
		$-2.00 \leq w_X \leq -0.33$	$\Omega_{m0} = 0.33$ $\Omega_{k0} = -0.1$	$0.30 \leq \Omega_{m0} \leq 0.36$ $-0.29 \leq \Omega_{k0} \leq 0.00$	$0.28 \leq \Omega_{m0} \leq 0.39$ $-0.52 \leq \Omega_{k0} \leq 0.09$
	$\phi$ CDM	$-0.5 \leq \Omega_{k0} \leq 0.5$	$\Omega_{m0} = 0.33$ $\alpha = 0.93$	$0.30 \leq \Omega_{m0} \leq 0.36$ $0.01 \leq \alpha \leq 1.41$	$0.28 \leq \Omega_{m0} \leq 0.39$ $0.01 \leq \alpha \leq 1.81$
		$0.01 \leq \Omega_{m0} \leq 0.99$	$\Omega_{k0} = -0.21$ $\alpha = 0.92$	$-0.38 \leq \Omega_{k0} \leq -0.10$ $0.01 \leq \alpha \leq 1.42$	$-0.48 \leq \Omega_{k0} \leq 0.00$ $0.01 \leq \alpha \leq 1.84$
		$0.01 \leq \alpha \leq 5$	$\Omega_{m0} = 0.33$ $\Omega_{k0} = -0.22$	$0.30 \leq \Omega_{m0} \leq 0.36$ $-0.39 \leq \Omega_{k0} \leq -0.10$	$0.28 \leq \Omega_{m0} \leq 0.39$ $-0.48 \leq \Omega_{k0} \leq -0.01$
$73.24 \pm 1.74$	XCDM	$-0.7 \leq \Omega_{k0} \leq 0.20$	$\Omega_{m0} = 0.32$ $w_X = -1.32$	$0.29 \leq \Omega_{m0} \leq 0.35$ $-1.58 \leq w_X \leq -1.13$	$0.27 \leq \Omega_{m0} \leq 0.38$ $-1.85 \leq w_X \leq -0.95$
		$0.20 \leq \Omega_{m0} \leq 0.45$	$\Omega_{k0} = -0.01$ $w_X = -1.32$	$-0.10 \leq \Omega_{k0} \leq 0.05$ $-1.58 \leq w_X \leq -1.13$	$-0.19 \leq \Omega_{k0} \leq 0.11$ $-1.85 \leq w_X \leq -0.95$
		$-2.00 \leq w_X \leq -0.33$	$\Omega_{m0} = 0.32$ $\Omega_{k0} = -0.01$	$0.29 \leq \Omega_{m0} \leq 0.35$ $-0.10 \leq \Omega_{k0} \leq 0.05$	$0.27 \leq \Omega_{m0} \leq 0.38$ $-0.19 \leq \Omega_{k0} \leq 0.11$
	$\phi$ CDM	$-0.5 \leq \Omega_{k0} \leq 0.5$	$\Omega_{m0} = 0.32$ $\alpha = 0.01$	$0.29 \leq \Omega_{m0} \leq 0.35$ $0.01 \leq \alpha \leq 0.48$	$0.27 \leq \Omega_{m0} \leq 0.38$ $0.01 \leq \alpha \leq 1.12$
		$0.01 \leq \Omega_{m0} \leq 0.99$	$\Omega_{k0} = -0.17$ $\alpha = 0.01$	$-0.30 \leq \Omega_{k0} \leq -0.11$ $0.01 \leq \alpha \leq 0.48$	$-0.45 \leq \Omega_{k0} \leq -0.04$ $0.01 \leq \alpha \leq 1.13$
		$0.01 \leq \alpha \leq 5$	$\Omega_{m0} = 0.32$ $\Omega_{k0} = -0.17$	$0.29 \leq \Omega_{m0} \leq 0.35$ $-0.30 \leq \Omega_{k0} \leq -0.10$	$0.27 \leq \Omega_{m0} \leq 0.38$ $-0.45 \leq \Omega_{k0} \leq -0.04$

Ding X., Biesiada M., Cao S., Li Z., Zhu Z.-H., 2015, *ApJ*, **803**, L22  
Eisenstein D. J., Hu W., 1998, *ApJ*, **496**, 605  
Farooq M. O., 2013, PhD thesis, Kansas State U. ([arXiv:1309.3710](#))  
Farooq O., Ratra B., 2013, *ApJ*, **766**, L7  
Farooq O., Crandall S., Ratra B., 2013, *Physics Letters B*, **726**, 72  
Farooq O., Mania D., Ratra B., 2015, *Ap&SS*, **357**, 11  
Farooq O., Ranjeet Madiyar F., Crandall S., Ratra B., 2017, *ApJ*, **835**, 26  
Fernández Arenas D., et al., 2018, *MNRAS*, **474**, 1250  
Font-Ribera A., et al., 2014, *J. Cosmology Astropart. Phys.*, **5**, 027  
Gómez-Valent A., Amendola L., 2018, *J. Cosmology Astropart. Phys.*, **4**, 051  
Gómez-Valent A., Solà J., 2017, *EPL (Europhysics Letters)*, **120**, 39001  
Gómez-Valent A., Solà J., 2018, preprint, ([arXiv:1801.08501](#))  
Gott III J. R., 1982, *Nature*, **295**, 304  
Gott III J. R., Vogeley M. S., Podariu S., Ratra B., 2001, *ApJ*, **549**, 1  
Haridasu B. S., Luković V. V., Vittorio N., 2017, preprint, ([arXiv:1711.03929](#))  
Haridasu B. S., Luković V. V., Moresco M., Vittorio N., 2018, preprint, ([arXiv:1805.03595](#))  
Hawking S. W., 1984, *Nuclear Physics B*, **239**, 257  
Hogg D. W., 1999, ArXiv Astrophysics e-prints,  
Jesus J. F., Holanda R. F. L., Pereira S. H., 2017, preprint, ([arXiv:1712.01075](#))  
L'Huillier B., Shafieloo A., 2017, *J. Cosmology Astropart. Phys.*, **1**, 015  
Liddle A. R., 2007, *MNRAS*, **377**, L74  
Lin W., Ishak M., 2017, *Phys. Rev. D*, **96**, 083532

Luković V. V., Haridasu B. S., Vittorio N., 2018, preprint, ([arXiv:1801.05765](#))  
Martin J., 2012, *Comptes Rendus Physique*, **13**, 566  
Mehrabi A., Basilakos S., 2018, preprint, ([arXiv:1804.10794](#))  
Mitra S., Choudhury T. R., Ratra B., 2017, preprint, ([arXiv:1712.00018](#))  
Moresco M., 2015, *MNRAS*, **450**, L16  
Moresco M., et al., 2012, *J. Cosmology Astropart. Phys.*, **8**, 006  
Moresco M., et al., 2016, *J. Cosmology Astropart. Phys.*, **5**, 014  
Ooba J., Ratra B., Sugiyama N., 2017a, preprint, ([arXiv:1707.03452](#))  
Ooba J., Ratra B., Sugiyama N., 2017c, preprint, ([arXiv:1712.08617](#))  
Ooba J., Ratra B., Sugiyama N., 2017b, preprint, ([arXiv:1710.03271](#))  
Ooba J., Ratra B., Sugiyama N., 2018, preprint, ([arXiv:1802.05571](#))  
Park C.-G., Ratra B., 2018a, preprint, ([arXiv:1803.05522](#))  
Park C.-G., Ratra B., 2018b, preprint, ([arXiv:1801.00213](#))  
Pavlov A., Westmoreland S., Saaidi K., Ratra B., 2013, *Phys. Rev. D*, **88**, 123513  
Pavlov A., Farooq O., Ratra B., 2014, *Phys. Rev. D*, **90**, 023006  
Peebles P. J. E., 1984, *ApJ*, **284**, 439  
Peebles P. J. E., Ratra B., 1988, *ApJ*, **325**, L17  
Planck Collaboration, Ade P. A. R., Aghanim N., Arnaud M., et al. 2016, *A&A*, **594**, A13  
Rana A., Jain D., Mahajan S., Mukherjee A., 2017, *J. Cosmology Astropart. Phys.*, **3**, 028  
Ratra B., 1985, *Phys. Rev. D*, **31**, 1931  
Ratra B., 2017, *Phys. Rev. D*, **96**, 103534  
Ratra B., Peebles P. J. E., 1988, *Phys. Rev. D*, **37**, 3406



- Ratra B., Peebles P. J. E., 1994, *ApJ*, 432, L5
- Ratra B., Peebles P. J. E., 1995, *Phys. Rev. D*, 52, 1837
- Ratra B., Vogeley M. S., 2008, *PASP*, 120, 235
- Ratsimbazafy A. L., Loubser S. I., Crawford S. M., Cress C. M., Bassett B. A., Nichol R. C., Väisänen P., 2017, *MNRAS*, 467, 3239
- Riess A. G., et al., 2016, *ApJ*, 826, 56
- Rigault M., et al., 2015, *ApJ*, 802, 20
- Ross A. J., Samushia L., Howlett C., Percival W. J., Burden A., Manera M., 2015, *MNRAS*, 449, 835
- Sahni V., Shafieloo A., Starobinsky A. A., 2014, *ApJ*, 793, L40
- Samushia L., Ratra B., 2010, *ApJ*, 714, 1347
- Samushia L., Chen G., Ratra B., 2007, preprint, ([arXiv:0706.1963](https://arxiv.org/abs/0706.1963))
- Sangwan A., Tripathi A., Jassal H. K., 2018, preprint, ([arXiv:1804.09350](https://arxiv.org/abs/1804.09350))
- Simon J., Verde L., Jimenez R., 2005, *Phys. Rev. D*, 71, 123001
- Sola Peracaula J., de Cruz Perez J., Gomez-Valent A., 2016, preprint, ([arXiv:1606.00450](https://arxiv.org/abs/1606.00450))
- Solà J., Gómez-Valent A., de Cruz Pérez J., 2015, *ApJ*, 811, L14
- Sola J., de Cruz Perez J., Gomez-Valent A., 2017a, preprint, ([arXiv:1703.08218](https://arxiv.org/abs/1703.08218))
- Solà J., Gómez-Valent A., de Cruz Pérez J., 2017b, *Modern Physics Letters A*, 32, 1750054
- Solà J., Gómez-Valent A., de Cruz Pérez J., 2017c, *Physics Letters B*, 774, 317
- Solà J., Gómez-Valent A., de Cruz Pérez J., 2017d, *ApJ*, 836, 43
- Stern D., Jimenez R., Verde L., Kamionkowski M., Stanford S. A., 2010, *J. Cosmology Astropart. Phys.*, 2, 008
- Wang Y., Xu L., Zhao G.-B., 2017, *ApJ*, 849, 84
- Wei J.-J., Wu X.-F., 2017, *ApJ*, 838, 160
- Yashar M., Bozek B., Abrahamse A., Albrecht A., Barnard M., 2009, *Phys. Rev. D*, 79, 103004
- Yu H., Wang F. Y., 2016, *ApJ*, 828, 85
- Yu H., Ratra B., Wang F.-Y., 2018, *ApJ*, 856, 3
- Zhai Z., Blanton M., Slosar A., Tinker J., 2017, *ApJ*, 850, 183
- Zhang C., Zhang H., Yuan S., Liu S., Zhang T.-J., Sun Y.-C., 2014, *Research in Astronomy and Astrophysics*, 14, 1221
- Zhang Y.-C., Zhang H.-Y., Wang D.-D., Qi Y.-H., Wang Y.-T., Zhao G.-B., 2017a, *Research in Astronomy and Astrophysics*, 17, 050
- Zhang B. R., Childress M. J., Davis T. M., Karpenka N. V., Lidman C., Schmidt B. P., Smith M., 2017b, *MNRAS*, 471, 2254
- Zhao G.-B., et al., 2017, *Nature Astronomy*, 1, 627
- Zheng X., Ding X., Biesiada M., Cao S., Zhu Z.-H., 2016, *ApJ*, 825, 17

This paper has been typeset from a  $\text{\TeX}/\text{\LaTeX}$  file prepared by the author.